Ion permeation in K^+ channels occurs by direct Coulomb knock-on

David A. Köpfer *et al.*

Science **346**, 352 (2014);
DOI: 10.1126/science.1254840

or in the probability of a tornado given favorable environmental conditions, is involved. Determining the relative contribution will require the continued development of relationships between environments and events (*11*, *12*), which will depend on the quality of high-resolution reanalysis products of the atmosphere (*13*–*15*). How such a change would relate to the increase in global temperature, if it relates at all, is unknown at this time. Nevertheless, if the variability continues to increase, it could lead to an even greater concentration of tornadoes on fewer days.

REFERENCES AND NOTES

1. C. A. Doswell III, H. E. Brooks, N. Dotzek, *Atmos. Res.* **93**, 554–563 (2009).
2. S. M. Verbout, H. E. Brooks, L. M. Leslie, D. M. Schultz, *Wea. Forecast.* **21**, 86–93 (2006).
3. IPCC, *Climate Change 2013: The Physical Science Basis. Contribution of Working Group I to the Fifth Assessment Report of the Intergovernmental Panel on Climate Change*, T. F. Stocker *et al.*, Eds. (Cambridge Univ. Press, Cambridge, 2013).
4. H. E. Brooks, *Atmos. Res.* **123**, 129–138 (2013).
5. H. E. Brooks, J. W. Lee, J. P. Craven, *Atmos. Res.* **67-68**, 73–94 (2003).
6. R. J. Trapp *et al.*, *Proc. Natl. Acad. Sci. U.S.A.* **104**, 19719–19723 (2007).
7. R. J. Trapp, N. S. Diffenbaugh, A. Gluhovsky, *Geophys. Res. Lett.* **36**, L01703 (2009).
8. N. S. Diffenbaugh, M. Scherer, R. J. Trapp, *Proc. Natl. Acad. Sci. U.S.A.* **110**, 16361–16366 (2013).
9. E. N. Rasmussen, D. O. Blanchard, *Wea. Forecast.* **13**, 1148–1164 (1998).
10. J. P. Craven, H. E. Brooks, *Nat. Wea. Digest* **28**, 13–24 (2004).
11. C. M. Shafer, A. E. Mercer, C. A. Doswell III, M. B. Richman, L. M. Leslie, *Mon. Weather Rev.* **137**, 1250–1271 (2009).
12. C. M. Shafer, A. E. Mercer, M. B. Richman, L. M. Leslie, C. A. Doswell III, *Wea. Forecast.* **27**, 809–831 (2012).
13. E. N. Kalnay *et al.*, *Bull. Am. Meteorol. Soc.* **77**, 437–471 (1996).
14. S. M. Uppala *et al.*, *Q. J. R. Meteorol. Soc.* **131**, 2961–3012 (2005).
15. G. P. Compo, J. S. Whitaker, P. D. Sardeshmukh, *Bull. Am. Meteorol. Soc.* **87**, 175–190 (2006).

ACKNOWLEDGMENTS

The scientific results and conclusions, as well as any views or opinions expressed herein, are those of the authors and do not necessarily reflect the views of NOAA or the Department of Commerce. G.W.C. carried out quality control on the dataset, H.E.B. performed primary analyses, and P.T.M. performed additional analyses and prepared figures.

SUPPLEMENTARY MATERIALS

www.sciencemag.org/content/346/6207/349/suppl/DC1
Materials and Methods
SupplementaryText
Fig. S1
Table S1

16 June 2014; accepted 11 September 2014
10.1126/science.1257460

ION CHANNELS

Ion permeation in K^+ channels occurs by direct Coulomb knock-on

David A. Köpfer,[1]† Chen Song,[2]*† Tim Gruene,[3] George M. Sheldrick,[3] Ulrich Zachariae,[4,5]*‡ Bert L. de Groot[1]*‡

Potassium channels selectively conduct K^+ ions across cellular membranes with extraordinary efficiency. Their selectivity filter exhibits four binding sites with approximately equal electron density in crystal structures with high K^+ concentrations, previously thought to reflect a superposition of alternating ion- and water-occupied states. Consequently, cotranslocation of ions with water has become a widely accepted ion conduction mechanism for potassium channels. By analyzing more than 1300 permeation events from molecular dynamics simulations at physiological voltages, we observed instead that permeation occurs via ion-ion contacts between neighboring K^+ ions. Coulomb repulsion between adjacent ions is found to be the key to high-efficiency K^+ conduction. Crystallographic data are consistent with directly neighboring K^+ ions in the selectivity filter, and our model offers an intuitive explanation for the high throughput rates of K^+ channels.

Potassium (K^+) channels play fundamental roles in almost all cell types. They are essential elements in cellular electric excitability and help maintain the resting potential in non-excitable cells. Their universality is based on a unique combination of strong selectivity for K^+ ions and near–diffusion-limited permeation efficiency (*1*). Common to all K^+ channels is the highly conserved K^+ selectivity filter (SF), which underlies both their exquisite K^+ selectivity and high conduction rates. A wealth of K^+ channel structural information has been acquired since 1998 (*2*). The structures revealed that the SF is formed at the interface of four channel subunits, each contributing a linearly extended backbone of five or six residues (Fig. 1A, left), the carbonyl groups of which point into a four-fold symmetric narrow pore (*2*). This arrangement generates four equidistant K^+ binding sites (S_1 to S_4; Fig. 1A, right) (*2*–*5*).

Anomalous scattering data from the bacterial K^+ channel KcsA from *Streptomyces lividans*, in whose SF K^+ ions were replaced with Tl^+, had originally been interpreted as a superposition of two states, each displaying occupation with two alkali ions alternating with water (Fig. 1B) (*4*). This interpretation still forms the basis for the commonly accepted K^+ conduction mechanism, which suggests cotranslocation of ions with water (*4*, *6*–*9*) (fig. S1). Any possible closer grouping of K^+ ions had been excluded owing to the expectation that the electrostatic repulsion between the ions would prohibit such an arrangement (*4*, *9*), although it was noted that geometrically, the ions could fit in the filter side by side (*9*, *10*). The notion of K^+-water cotranslocation has been applied to other K^+ channels (*11*–*14*), and similar mechanisms have been reported in equilibrium (*10*, *15*–*18*) and non-equilibrium (*19*–*21*) simulation studies. In most of these, biasing restraints were applied on the filter and/or supraphysiological transmembrane voltages were applied to elicit ion transfer (*19*–*21*). However, alternative computational studies demonstrated that multiple pathways may exist, including mechanisms that exhibit close ionic contacts and display similar free energy barriers to K^+ permeation (*18*, *22*, *23*). It has thus remained unclear which mechanism of K^+ permeation predominates under physiological conditions.

Table 1. Occupancy refinement of Tl^+ in the KcsA structure (PDB ID 1r3j) and K^+ in the MthK structure (PDB ID 3ldc), respectively. The absolute occupancy was determined with SHELXL, which allowed for an estimation of the absolute error. Values greater than one are caused by the correlation between occupancies and *B* values. As an independent cross-validation, we calculated the relative occupancies based solely on the anomalous signal using SHELXD.

Binding site	KcsA, refinement of Tl^+			MthK, refinement of K^+	
	Residue ID	Absolute occupancy	Relative occupancy	Residue ID	Absolute occupancy
S_1	C401	1.02 ± 0.04	1.0	A1	0.92 ± 0.07
S_2	C402	0.93 ± 0.03	0.9	A2	0.80 ± 0.07
S_3	C403	0.92 ± 0.04	0.9	A3	1.00 ± 0.09
S_4	C404	0.99 ± 0.04	1.0	A4	1.00 ± 0.09

[1]Biomolecular Dynamics Group, Max Planck Institute for Biophysical Chemistry, 37077 Göttingen, Germany. [2]Department of Biochemistry, University of Oxford, Oxford OX1 3QU, UK. [3]Department of Structural Chemistry, University of Göttingen, 37077 Göttingen, Germany. [4]School of Engineering, Physics and Mathematics, University of Dundee, Dundee DD1 4HN, UK. [5]College of Life Sciences, University of Dundee, Dundee DD1 5EH, UK.
***Corresponding author. E-mail: sc3210@gmail.com (C.S.); u.zachariae@dundee.ac.uk (U.Z.); bgroot@gwdg.de (B.L.d.G.)**
†These authors contributed equally to this work. ‡These authors contributed equally to this work.

Enabled by the recent availability of K^+ crystal structures with an open gate (*24*) and methods to simulate ion flux driven by transmembrane ion gradients (*25*), we set out to investigate the molecular mechanism of ion transfer across the K^+ channel SF from first principles. We performed atomistic molecular dynamics (MD) simulations of KcsA [Protein Data Bank (PDB) IDs 3f5w, 3fb7, and 1k4c] under sustained transmembrane potentials, evoked by K^+ ion gradients, to study the molecular basis of K^+ conduction efficiency in the physiological voltage range (Fig. 1C). The simulations were repeated in the archaeal MthK channel from *Methanobacterium thermoautotrophicum* (PDB ID 3ldc) and the eukaryotic $K_v1.2$-$K_v2.1$ chimeric channel (PDB ID 2r9r) (fig. S4). In total, we recorded more than 1300 spontaneous K^+ permeation events within a simulation time of ~50 μs.

At KCl concentrations of 400 mM, 200 mM, and 10 mM, we recorded the number of permeating ions as a function of time, where the slope of the curves reflects ion current (Fig. 1D). The simulated currents under positive potentials are in good agreement with experimentally reported values (up to a factor of ~2, similar to the experimental range of variation). We found that sustained currents were restricted to states displaying adjacent K^+ ions in the SF. These invariably involved a K^+ ion pair at binding sites S_2 and S_3 in the SF. One ion bound near S_0, frequently exchanging with ions from the bulk solution (Fig. 1E), such that S_1 was left vacant. Individual outward permeation events were initiated by intracellular K^+ ions entering into the internal channel cavity at binding site S_{cav}. Translocation of the central ions in the SF at S_3 and S_2 started when a water molecule at S_4 left to generate a vacancy (Fig. 1, F and G).

At the core of the permeation mechanism is a fast, concerted motion of the three ions at binding sites S_{cav}, S_3, and S_2, triggered by positional fluctuations of the incoming K^+ ion between S_{cav} and S_4 (Fig. 1H). These motions repeatedly reduce its distance to the ion pair at S_3 and S_2. A subsequent "knock-on" between the ion at S_4 and the S_3-S_2 ion pair ultimately leads to a progression of the central ion pair to S_2 and S_1 (Fig. 1I) and to further ion transfers from S_1 to S_0 and from S_4 to S_3 (Fig. 1J). These final rearrangements complete the transition by reestablishing the initial occupancy pattern of the SF (Fig. 1E). We observed the direct knock-on mechanism in simulations of three KcsA crystal structures (PDB IDs 3f5w, 3fb7, and 1k4c), MthK (PDB ID 3ldc), and the voltage-gated channel chimera $K_v1.2$-$K_v2.1$ (PDB ID 2r9r), independently of the force fields and water models used (fig. S4 and tables S1 and S2).

Our finding that direct ion contacts underpin the most efficient K^+ permeation route in K^+ channels contrasts with the commonly accepted transport mechanism, which is based on alternating ion and water occupation inside the SF. Similar direct cation-cation contacts have so far mainly been detected in concentrated salt solutions (*26*). The accepted mechanism has predominantly been inferred from channel crystallographic data, among which the anomalous data of Tl^+ ions in the KcsA SF (PDB ID 1r3j) played a particularly important role (*4*). We were therefore interested in whether our simulation results were compatible with the experimental data. Because the original interpretation of the anomalous electron density map may contain potential drawbacks (such as a degree of dependence on the quality of the refined model from which phases are calculated), we used the program SHELXD (*27*) to determine Tl^+ occupancies in KcsA solely against anomalous data. This analysis established the relative occupancies to be equal among all four ions, within experimental error. The absolute occupancy was refined by SHELXL (*28*) (Table 1). In addition, K^+ occupancies

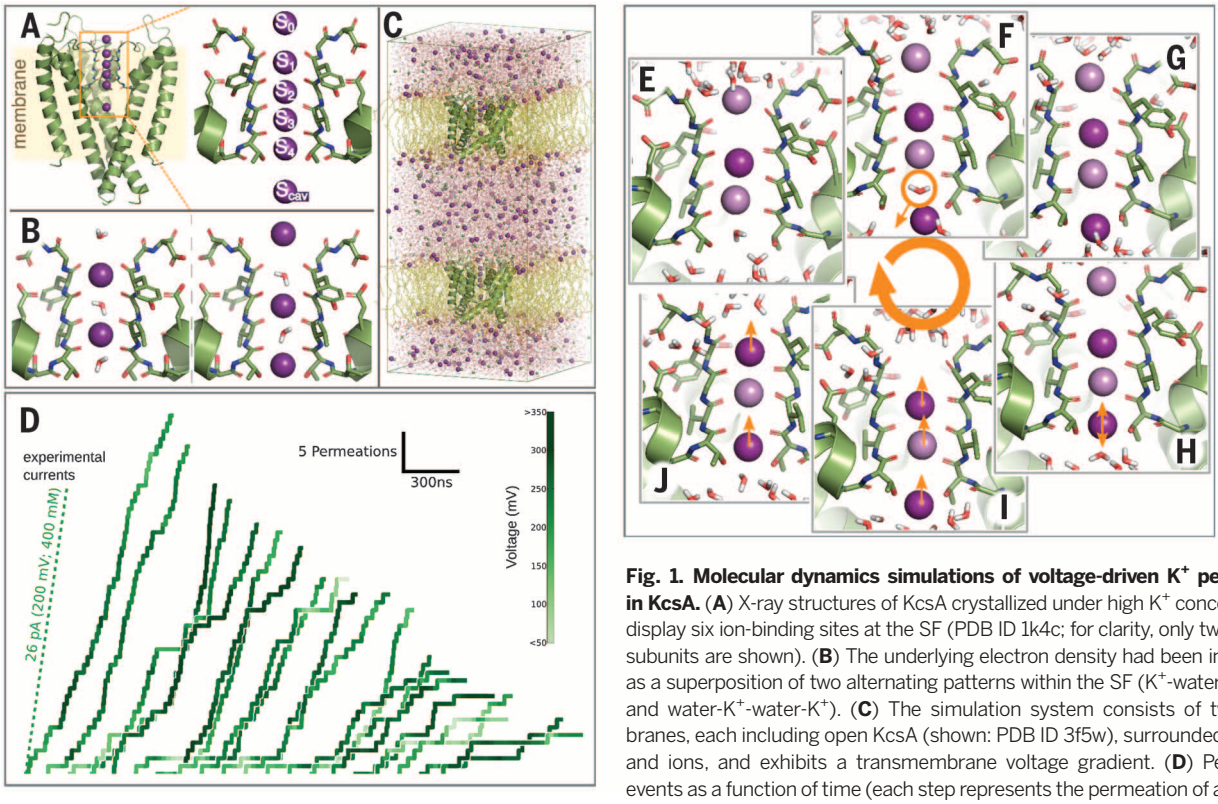

Fig. 1. Molecular dynamics simulations of voltage-driven K^+ permeation in KcsA. (**A**) X-ray structures of KcsA crystallized under high K^+ concentrations display six ion-binding sites at the SF (PDB ID 1k4c; for clarity, only two or three subunits are shown). (**B**) The underlying electron density had been interpreted as a superposition of two alternating patterns within the SF (K^+-water-K^+-water and water-K^+-water-K^+). (**C**) The simulation system consists of two membranes, each including open KcsA (shown: PDB ID 3f5w), surrounded by water and ions, and exhibits a transmembrane voltage gradient. (**D**) Permeation events as a function of time (each step represents the permeation of a single K^+ ion) over 20 individual simulations at 400 mM KCl (set I; see table S1) and in comparison with experimentally measured ion currents [dashed line, data from (*36*)]. The slope of each curve denotes computed or experimental current. The transmembrane voltage measured in experiments and simulations is color-coded from light to dark green. (**E** to **J**) Observed mechanism and sequence of events during K^+ translocation. The most frequent ion configuration under voltage contains two K^+ ions at S_2 and S_3 and a more loosely bound ion at S_0, leaving a vacancy at S_1 (E). Permeation starts when a K^+ ion enters the cavity and binds to S_{cav} (F). Upon displacement of a water molecule (G), translocation of the central ions is triggered by fluctuations of the incoming ion between S_{cav} and S_4, coinciding with release of K^+ from S_0 into the solution (H). Ions at S_3 and S_2 advance in a fast, concerted transition (I), followed by the movement of ions at S_4 and S_1 (J), reestablishing the initial configuration (E).

were refined for MthK (PDB ID 3ldc) (*29*) and Kir3.1 (PDB ID 2qks) (*30*) (Table 1 and tables S4 and S5). We consistently find high values close to unit occupancy that are consistent with the interpretation that close contacts between alkali ions occur in the SF. These contacts were identified as the key to efficient conduction in our MD simulations. Water molecules do not seem to be necessary to separate alkali ions in the filter in order to shield them from repulsion. As previously suggested, and as directly observed in our simulations under transmembrane voltage, ion conduction in K^+ channels "in action" relies on frequent transitions between substates of different ion occupation, whereas open-activated channel states under crystalline conditions are thought to be characterized by the presence of electron density at all four SF positions (*31*). Accordingly, without applied voltage and at reduced temperature, the SF occupancy seen in our simulations converges to that observed in the crystal structures (PDB IDs 1k4c and 3ldc) (fig. S2).

We next investigated whether the basic physical principles of ion translocation in single file predetermine close ion-ion contacts to drive efficient permeation. We modeled the fundamental ion translocation event as Brownian diffusion in a periodic one-dimensional potential, reflecting the sequence of ion-water binding sites in the SF (Fig. 2 and supplementary materials). By testing various occupation patterns and a range of membrane voltages, we found that configurations with direct contacts between ions consistently gave rise to markedly higher transfer rates than water-separated patterns in our Brownian dynamics simulations. These results were independent of the ion and water models used and of the details of the potential (fig. S6 and supplementary materials). Under physiologically relevant voltages, fully ion-occupied systems showed a conductance of ~80 pS, whereas those with alternating ion and water occupancy displayed only little permeation, further decreasing with increasing water content (Fig. 2). Hence, a simple physical model of ion transfer through a confined pore with multiple binding sites already predicts ion-ion contacts to enhance, and the presence of uncharged species to impede, ion permeation.

Together with the results from our MD simulations, the data suggest that water is not cotranslocated with K^+ to a large degree in open-activated KcsA. This is seemingly in conflict with the ion/water cotranslocation ratio derived from measurements of water translocation through KcsA (*32*–*35*). However, these experiments were based on the application of high osmotic gradients. Water permeation as a result of an applied osmotic pressure is likely to lead to ion-depleted SF states in which individual ions are only occasionally dragged along by permeating water molecules, whereas bound ions are reported to completely block water flux (*33*, *34*). Such ion-depleted, and water-permeable, filter states are therefore likely markedly different from the ion-conductive states at higher ion occupancy considered by crystallography and in our MD simulations.

The agreement among the multiple approaches we used to study ion flux in K^+ channels suggests a consensus mechanism of ion permeation across the SF. Figure 3 displays a schematic potential landscape in the SF according to the main observations made in our simulations (Fig. 3A, gray). In the resting state under physiological membrane voltage, two K^+ ions bind stably to S_2 and S_3 (Fig. 3A, purple). The height of the energy barrier (red) prevents transfer of K^+ from S_2 to S_1. As K^+ enters into S_{cav} and progresses to S_4, Coulomb repulsion with the central ions leads to their relative energetic destabilization (Fig. 3, B and C). This Coulomb interaction also lowers the permeation barrier between S_2 and S_1 (Fig. 3C). As a result, productive translocation of the ion at S_2 can occur (Fig. 3D). Subsequently, translocation from S_3 to S_2 lowers the potential energy of the ion at S_4, while simultaneously the energy of the ion at S_1 is increased (Fig. 3E, red arrows). Owing to the new potential energy surface, the initial ion configuration is then recovered by transfer from S_4 to S_3 and exit of the ion at S_1 from the SF (Fig. 3F). This cycle constitutes a full conduction

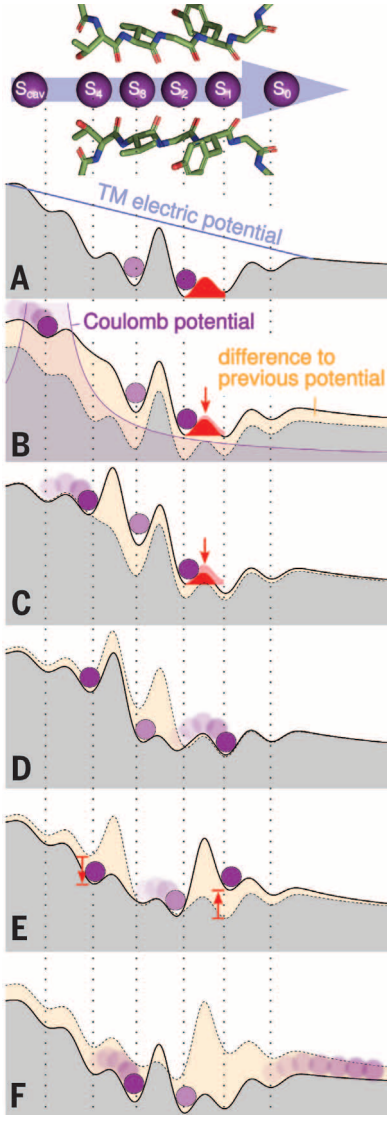

Fig. 3. Energetic basis and mechanism of ion permeation in the KcsA selectivity filter. (**A**) Potential landscape (gray) of the steady-state situation with K^+ simultaneously bound in S_2 and S_3 (purple) and a transmembrane (TM) electric potential attracting cations toward the extracellular face (blue). (**B**) An incoming K^+ ion binding to S_{cav} alters the potential of the ions at S_2 and S_3 as a result of Coulomb repulsion (magenta), raising their free energy with respect to the bulk and lowering the barrier for the ions at S_3 and S_2. (**C** and **D**) Subsequent binding of the incoming ion to S_4 (C) finally reduces the barrier sufficiently for the ion at S_2 to advance to S_1 (D). (**E**) The strong destabilization of the ion at S_1 is simultaneous with an increase in stabilization of the incoming ion at S_4 (red arrows), triggered by the transfer of the central ion to S_2. (**F**) In the last step, the ion at S_4 binds to S_3 while the ion at S_1 leaves the SF, thereby recovering the original state.

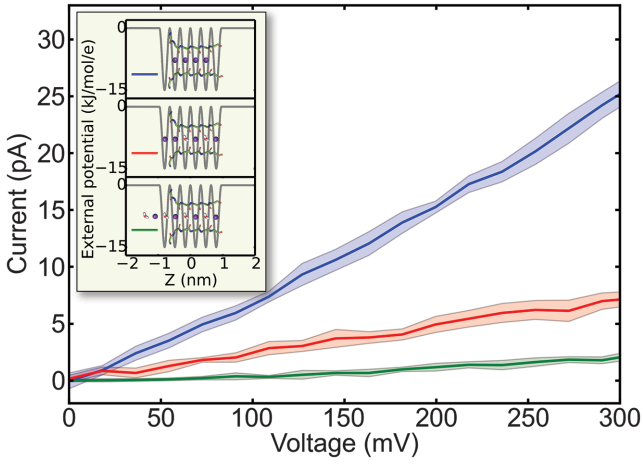

Fig. 2. Brownian dynamics simulations of K^+ ions and water across a repetitive well potential. Potential energy minima represent ion or water binding sites in the SF (insets). Approximately equal binding site affinity for each species, and hence potential depth, is implicitly assumed in the accepted ion-water cotranslocation model. An electric field was applied from left to right. The highest ionic current is seen when K^+ ions are bound in adjacent binding sites (blue line). When direct ion-ion contacts are only occasionally allowed (red line), the current decreases by ~70%. The canonical K^+-water-K^+-water pattern reduces the maximal current by an order of magnitude (green line).

step. Notably, the free energy required to destabilize binding at S_2 ultimately stems from the binding energy of the incoming ion, best seen during the transition of the central ion (Fig. 3E, red arrows).

The proposed mechanism predicts an important experimental characteristic of K^+ channels. Because the rate of K^+ ions leaving the SF at the extracellular side is determined by the rate with which incoming intracellular ions arrive at the filter (movie S1), our model inherently implies that K^+ channels are diffusion-limited as long as an ion pair occupies the inner SF binding sites. We therefore recorded the occupancy of the inner SF sites under varying K^+ concentrations. Indeed, we found that ions occupy these positions over a broad range of concentrations from 10 mM to 400 mM (fig. S3). Taken together, our model thus not only accounts for the diffusion control of K^+ channels, but also explains the wide linear regime of K^+ channel conductance above ~10 mM K^+ (*9*), which is a prerequisite for robust K^+ channel function under variable external conditions.

Our permeation model for ion transfer in K^+ channels at physiological voltages relies on repulsive Coulomb interactions between adjacent ions in the SF as the main driver for conduction near the diffusion limit (Fig. 3). In re-investigating several K^+ channel structures, we found direct ionic contacts to be compatible with the available crystallographic data. The results presented above demonstrate that these direct contacts are not energetically prohibitive. Rather, they serve to enhance ion flux to the maximum attainable speed over a broad range of concentrations.

REFERENCES AND NOTES

1. B. Hille, *Ion Channels of Excitable Membranes* (Sinauer, Sunderland, MA, ed. 3, 2001).
2. D. A. Doyle *et al.*, *Science* **280**, 69–77 (1998).
3. Y. Zhou, J. H. Morais-Cabral, A. Kaufman, R. MacKinnon, *Nature* **414**, 43–48 (2001).
4. Y. Zhou, R. MacKinnon, *J. Mol. Biol.* **333**, 965–975 (2003).
5. L. G. Cuello *et al.*, *Nature* **466**, 272–275 (2010).
6. C. Domene, M. S. P. Sansom, *Biophys. J.* **85**, 2787–2800 (2003).
7. A. L. Hodgkin, R. D. Keynes, *J. Physiol.* **128**, 61–88 (1955).
8. C. Miller, *Nature* **414**, 23–24 (2001).
9. J. H. Morais-Cabral, Y. Zhou, R. MacKinnon, *Nature* **414**, 37–42 (2001).
10. J. Åqvist, V. Luzhkov, *Nature* **404**, 881–884 (2000).
11. L. Ceccarini, M. Masetti, A. Cavalli, M. Recanatini, *PLOS ONE* **7**, e49017 (2012).
12. F. Khalili-Araghi, E. Tajkhorshid, K. Schulten, *Biophys. J.* **91**, L72–L74 (2006).
13. G. Yellen, *Nature* **419**, 35–42 (2002).
14. T. Lu *et al.*, *Nat. Neurosci.* **4**, 239–246 (2001).
15. S. Bernèche, B. Roux, *Biophys. J.* **78**, 2900–2917 (2000).
16. I. H. Shrivastava, M. S. P. Sansom, *Biophys. J.* **78**, 557–570 (2000).
17. T. Sumikama, S. Saito, I. Ohmine, *J. Phys. Chem. B* **110**, 20671–20677 (2006).
18. S. Bernèche, B. Roux, *Nature* **414**, 73–77 (2001).
19. M. Ø. Jensen *et al.*, *Proc. Natl. Acad. Sci. U.S.A.* **107**, 5833–5838 (2010).
20. M. Ø. Jensen, V. Jogini, M. P. Eastwood, D. E. Shaw, *J. Gen. Physiol.* **141**, 619–632 (2013).
21. K. Kasahara, M. Shirota, K. Kinoshita, *PLOS ONE* **8**, e56342 (2013).
22. S. Furini, C. Domene, *Proc. Natl. Acad. Sci. U.S.A.* **106**, 16074–16077 (2009).
23. P. W. Fowler, E. Abad, O. Beckstein, M. S. P. Sansom, *J. Chem. Theory Comput.* **9**, 5176–5189 (2013).
24. L. G. Cuello, V. Jogini, D. M. Cortes, E. Perozo, *Nature* **466**, 203–208 (2010).
25. C. Kutzner, H. Grubmüller, B. L. de Groot, U. Zachariae, *Biophys. J.* **101**, 809–817 (2011).
26. G. Hummer, D. M. Soumpasis, M. Neumann, *Mol. Phys.* **81**, 1155–1163 (1994).
27. C. B. Hübschle, G. M. Sheldrick, B. Dittrich, *J. Appl. Crystallogr.* **44**, 1281–1284 (2011).
28. G. M. Sheldrick, *Acta Crystallogr. A* **64**, 112–122 (2008).
29. S. Ye, Y. Li, Y. Jiang, *Nat. Struct. Mol. Biol.* **17**, 1019–1023 (2010).
30. M. Nishida, M. Cadene, B. T. Chait, R. MacKinnon, *EMBO J.* **26**, 4005–4015 (2007).
31. O. B. Clarke *et al.*, *Cell* **141**, 1018–1029 (2010).
32. M. Iwamoto, S. Oiki, *J. Neurosci.* **31**, 12180–12188 (2011).
33. T. Hoomann, N. Jahnke, A. Horner, S. Keller, P. Pohl, *Proc. Natl. Acad. Sci. U.S.A.* **110**, 10842–10847 (2013).
34. S. M. Saparov, P. Pohl, *Proc. Natl. Acad. Sci. U.S.A.* **101**, 4805–4809 (2004).
35. S. Imai, M. Osawa, K. Takeuchi, I. Shimada, *Proc. Natl. Acad. Sci. U.S.A.* **107**, 6216–6221 (2010).
36. M. LeMasurier, L. Heginbotham, C. Miller, *J. Gen. Physiol.* **118**, 303–314 (2001).

ACKNOWLEDGMENTS

We thank H. Sun and S. Wacker for simulations of $K_v1.2$, R. Sknepnek for assistance with HOOMD-blue, and H. Grubmüller, M.S.P. Sansom, P. Pohl, T. Graen, and K. Zeth for helpful discussions. Supported by the International Max Planck Research School for Biology and Complex Systems (D.A.K.), a Marie Curie Intra European Fellowship within the 7th European Community Framework Programme (C.S.), the Volkswagen Stiftung (via the Niedersachsenprofessur awarded to G.M.S.) (T.G.), the Scottish Universities' Physics Alliance (U.Z.), and the German research foundation DFG through SFB803 (B.L.d.G.).

SUPPLEMENTARY MATERIALS

www.sciencemag.org/content/346/6207/352/suppl/DC1
Materials and Methods
Figs. S1 to S6
Tables S1 to S14
Movie S1
References (*37*–*63*)

15 April 2014; accepted 27 August 2014
10.1126/science.1254840

ION CHANNELS

Structure and selectivity in bestrophin ion channels

Tingting Yang,[1] Qun Liu,[2] Brian Kloss,[3] Renato Bruni,[3] Ravi C. Kalathur,[3] Youzhong Guo,[1] Edda Kloppmann,[3,4] Burkhard Rost,[3,4] Henry M. Colecraft,[5] Wayne A. Hendrickson[1,2,3,5]*

Human bestrophin-1 (hBest1) is a calcium-activated chloride channel from the retinal pigment epithelium, where mutations are associated with vitelliform macular degeneration, or Best disease. We describe the structure of a bacterial homolog (KpBest) of hBest1 and functional characterizations of both channels. KpBest is a pentamer that forms a five-helix transmembrane pore, closed by three rings of conserved hydrophobic residues, and has a cytoplasmic cavern with a restricted exit. From electrophysiological analysis of structure-inspired mutations in KpBest and hBest1, we find a sensitive control of ion selectivity in the bestrophins, including reversal of anion/cation selectivity, and dramatic activation by mutations at the cytoplasmic exit. A homology model of hBest1 shows the locations of disease-causing mutations and suggests possible roles in regulation.

The human *BEST1* gene encodes a protein [human bestrophin-1 (hBest1)] that is highly expressed in retinal pigment epithelium (*1*–*4*). More than 120 distinct mutations in hBest1 have been identified that result in multiple retinal degeneration disorders (*5*–*11*), notably vitelliform macular degeneration or Best disease. Functionally, hBest1 was identified as a Cl^- channel that can be activated by Ca^{2+} (*8*, *12*, *13*), and most of the disease-causing mutations in hBest1 are point mutations that cause channel dysfunction (*8*, *12*, *14*–*16*). Thus, understanding the structure of the hBest1 channel holds value from both biological and biomedical perspectives.

The bestrophin family identified by hBest1 is distributed widely, with representatives in most metazoan animals, including four in humans, and also in other eukaryotes and in prokaryotes (*7*, *8*). The animal bestrophins are characterized by a highly conserved N-terminal domain that includes four predicted transmembrane helices (TMs) and diverse C-terminal domains that may be involved in protein-protein interactions (*8*, *12*, *15*, *17*). Bacterial bestrophins lack the variable C-terminal domain and are more divergent in the transmembrane portion. Using a structural genomics approach, we identified a homolog from *Klebsiella pneumoniae* (KpBest) that could be produced by recombinant expression for structural and functional characterization. The structure-based sequence alignment implies 14% identity between KpBest and hBest1 (fig. S1).

Initial crystals of detergent-solubilized KpBest diffracted poorly; however, constructs from a truncation series did yield suitable crystals. The initial structure was solved from one of these,

[1]Department of Biochemistry and Molecular Biophysics, Columbia University, New York, NY 10032, USA. [2]New York Structural Biology Center, Synchrotron Beamlines, Brookhaven National Laboratory, Upton, NY 11973, USA. [3]New York Consortium on Membrane Protein Structure, New York Structural Biology Center, 89 Convent Avenue, New York, NY 10027, USA. [4]Department of Informatics, Bioinformatics and Computational Biology, TUM (Technische Universität München), Garching 85748, Germany. [5]Department of Physiology and Cellular Biophysics, Columbia University, New York, NY 10032, USA.
***Corresponding author. E-mail: wayne@xtl.cumc.columbia.edu**